J Mater Sci (2011) 46:5519–5526
DOI 10.1007/s10853-011-5496-6

Mechanical properties of cellular solids produced from hollow stainless steel spheres

Siddhartha Roy · Alexander Wanner · Tilmann Beck · Thomas Studnitzky · Günter Stephani

Received: 3 January 2011 / Accepted: 21 March 2011 / Published online: 31 March 2011

Abstract Mechanical properties of cellular hollow sphere structures are studied in this work. The material was fabricated by coating the metallic powder slurry on expanded polystyrol (EPS) spheres, drying, forming under compression, debinding, and final sintering of the spheres to each other. Longitudinal elastic wave velocities were measured using ultrasound phase spectroscopy while compression tests were carried out up to a homologous temperature of 0.6. Dependence of the relative Young's modulus on the relative density is similar to conventional open-cell foams. Compression stress–strain plots show the three stages of elastic deformation, plateau, and densification. With increasing temperature the overall level of the compressive stress–strain plots shifts to lower stresses. The hollow sphere solids show slightly better high temperature strength in comparison to the base metal. However, due to the considerable scatter in the experimental data points, this improvement seems to be insignificant. Structural observations on samples deformed to within the plateau region clearly show the heterogeneous progress of deformation.

S. Roy (✉) · A. Wanner
Institut für Angewandte Materialien, Karlsruher Institut für Technologie, Kaiserstr. 12, 76131 Karlsruhe, Germanny
e-mail: siddhartha.roy@kit.edu

S. Roy
Department of Metallurgical Engineering and Materials Science, Indian Institute of Technology Bombay, Mumbai 400076, India

T. Beck
Forschungszentrum Jülich, 52428 Jülich, Germany

T. Beck
Institut für Werkstoffkunde I, Universität Karlsruhe (TH), Kaiserstr. 12, 76131 Karlsruhe, Germany

T. Studnitzky · G. Stephani
Fraunhofer Institute for Manufacturing Technology and Advanced Materials (IFAM), Winterbergstr. 28, 01277 Dresden, Germany

Introduction

Cellular metals like metallic foams are attractive because of their high stiffness to weight ratio, light weight, good energy absorbing capacity, etc. Potential applications of these materials include energy absorbing lightweight elements in automobiles, e.g., as heat exchangers or energy absorbing elements [1–6]. Based upon their geometrical structure, conventional foams may be classified as either open or closed-cell foams. Analytical models describing the mechanical properties of conventional foams have been proposed by Gibson and Ashby (denoted GA model in the following) [7]. These models show that closed-cell foams should exhibit significantly higher stiffness and strength than open-cell foams having the same relative density. However, due to the specific structural defects present in closed-cell structures, the actual mechanical properties shown by both of them in compression tests are similar [8]. Furthermore, due to their inherent structural heterogeneity, the mechanical properties of metallic foams show a large scatter.

In a continuous quest to fabricate high quality metal foams, cellular hollow sphere structures have been developed in last about one decade [9]. The individual hollow spheres can be joined by brazing or sintering. Advantages of these materials include: (a) the ability to fabricate cellular solids with controllable and reproducible geometrical parameters like sphere diameter, cell wall thickness, etc., (b) structural homogeneity, and (c) the ability to use both low and high melting point metals as the cell wall materials [10]. The number of experimental studies carried out up to now to

investigate the mechanical properties of these hollow sphere structures [10–13] is limited in comparison to conventional metallic foams. Numerous authors have tried to develop models to predict the mechanical properties of hollow sphere structures which have a specific regular arrangement of individual spheres. Using finite element method (FEM), Sanders and Gibson predicted the mechanical properties of hollow sphere foams having simple cubic (SC) [14], and FCC and BCC [8] arrangements. Their results showed that the mechanical properties of the SC structure lied between that of open and closed-cell foams, while the FCC structure in general showed highest mechanical properties. Subsequently, Gasser et al. [15] proposed an analytical model to predict the Young's modulus of hollow sphere structures having FCC arrangement of the spheres.

In the current work, hollow sphere structures made of stainless steel and having relative densities in the range of 0.05–0.12 are studied. The material was fabricated by coating the metallic powder slurry on expanded polystyrol (EPS) spheres, drying, forming under compression, debinding, and final sintering of the spheres to each other. Elastic behavior was characterized by measuring the velocity of longitudinal elastic waves using an ultrasound spectroscopy technique. Compression tests were carried out at room temperature and at high temperatures up to 730 °C, corresponding to a homologous temperature of 0.6 (homologous temperature is defined as the ratio of the actual temperature and the melting temperature in absolute scale. Melting range of the cell wall material AISI 316L lies within 1370–1400 °C [16]). Results are compared with theoretical predictions for open and closed-cell foams. Structural characterization of both non-deformed and deformed materials is carried out to thoroughly understand the damage mechanism.

Experimental procedure

Material and sample preparation

Only a brief description of the manufacturing route is given here and thorough description can be found in Ref. [2]. Hollow sphere structures were fabricated at Fraunhofer IFAM, Dresden, Germany following a powder metallurgical route. EPS spheres were first coated with a slurry containing AISI 316L powder and a binder material. The 316L powder had nominal grain size of a d50 of 5.6 μm and a d90 of 9.8 μm and the particles were spherical in shape. The slurry was based on polyvinylalcohol and additives. After drying, the coated spheres were formed under compression and subsequently they were sintered. Debinding temperature was 600 °C, while sintering was carried out at 1250 °C. Both debinding and sintering were carried out in hydrogen atmosphere. The EPS spheres and the binder material is removed in a debinding process and neck forms between individual hollow stainless steel spheres during this sintering process. Three different types of hollow sphere structures having different sphere diameters but similar sphere wall thicknesses were fabricated. The samples were cylindrical in shape and their dimensions are given in Table 1. All received samples were machined using electrical discharge machining (EDM) for better surface finishing for subsequent analysis. EDM was employed as it imparts negligible cutting force and so the spheres were not distorted.

Ultrasound phase spectroscopy

Ultrasound phase spectroscopy (UPS) was used to determine the longitudinal wave velocities along the length axis of each cylindrical sample. Only a brief overview of the method is given here and for thorough description we refer to Ref. [17]. In this technique continuous, sinusoidal, elastic waves are used for the measurements and the phase shift occurring as the wave passes through the specimen is recorded as a function of frequency. The measurements were accomplished using an electronic network analyzer (Advantest, model R3754A) and two identical broadband ultrasonic longitudinal wave (Panametrics model V101 with nominal central frequency 0.5 MHz and diameter 25.4 mm) transducers. These transducers were attached to the opposite sides of the samples with the help of a water soluble couplant. The phase and the amplitude spectra were recorded in the frequency range from 10 kHz to 1 MHz. In

Table 1 Description of the studied hollow sphere structure

Type	Nominal sample size (mm)	Sphere dia. (mm)	Cell wall thickness (μm)	Avg. density (kg/m^3)	Avg. relative density
A	Height: 22 Diameter: 22	3	50	459 ± 43	0.057 ± 0.005
B	Height: 22 Diameter: 22	2	50–70	843 ± 65	0.105 ± 0.008
C	Height: 22, 30 Diameter: 22	1.5	50	739 ± 30	0.09 ± 0.003

a non-dispersive medium, the velocity of the propagating wave can be determined by following the relation:

$$V = -2\pi L/m \quad (1)$$

where L is the sample length along the propagating direction and m is the slope of the straight line fitted to the phase-frequency spectrum. Once the wave velocity is measured, the respective elastic constants can be determined using the relation:

$$C_{ii} = \rho V^2 \quad (2)$$

where ρ is the sample density.

Compression test

An electromechanical testing machine Zwick 1494 was used for the compression tests. Samples were compressed between two parallel, flat punches made of fine ground hardened steel. All the experiments were carried out under velocity controlled mode. Strain was measured with the help of a linear variable differential transformer (LVDT) mounted on the bottom crosshead at an off-axis position adjacent to the specimen. This type of strain measurement device is ideal for the situation where a large amount of strain is to be measured. The tests were stopped when the limiting load was reached or at the point where the required amount of deformation was achieved. Compression tests were carried out at room temperature (RT), 230, 400, 560, and 730 °C. For the elevated temperature tests, the samples were heated to the required temperature by radiation heating in a tube furnace in normal atmosphere. The furnace was mounted between the two crossheads. Ni–Cr–Ni thermocouple was used to measure the temperature and the temperature was controlled using a PID controller. A small hole was drilled on the longitudinal surface of the cylindrical samples and the thermocouple was inserted into it. After the required temperature was achieved, the specimens were kept only under a preload of 100 N for 10 min before the actual compression test began. This was done to ensure that temperature was uniform throughout the sample before the compression test. Before experiment, the samples were coated with a high temperature black paint to enhance heat absorption.

Results and discussions

Structural characterization of as received samples

Figure 1 shows the macroscopic top view of one sample of Type B before EDM cut. Density of each sample was determined by measuring the mass and dimensions.

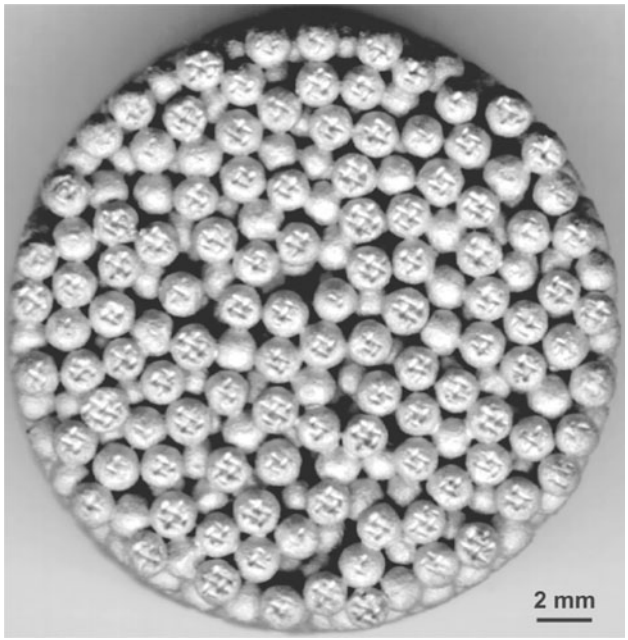

Fig. 1 Macroscopic *top view* of one sample of Type B

Average and standard deviation of density of all the samples within each material type are listed in Table 1. To calculate the relative density, the density of bulk AISI 316L was taken as 7900 kg/m^3 [16]. Average and standard deviation of the relative density within each material type are also listed in Table 1.

Figure 2 shows the typical light optical micrograph of a region where three adjacent spheres touch each other. Significant variation in the sizes of the austenite grains is observed and some of them cover the entire thickness of the cell walls. Three different kinds of porosities are observed in this micrograph. Following the nomenclature used by Friedl et al. [10], the pore space within individual spheres is known as macroporosity; the pore space between the spheres is known as mesoporosity, while the numerous small pores resulting from incomplete sintering, which are visible within the cell walls, are known as microporosity. Scott and Kilgour [18] measured the packing density of randomly packed identical spheres. They found that for different materials, the volume of pores between the spheres lies in the range of 37–43 vol.%. This can be taken as the amount of mesoporosity in the hollow sphere solids under study. To find the amount of microporosity within the cell walls, several optical micrographs similar to the one shown in Fig. 2 were analyzed. Ratio of the area of the pores within the cell walls and the total cell wall area was calculated and this was used as the volume fraction of micropores. Calculated this way, the amount of microporosity within the cell walls was found to be approximately 3–4 vol.%.

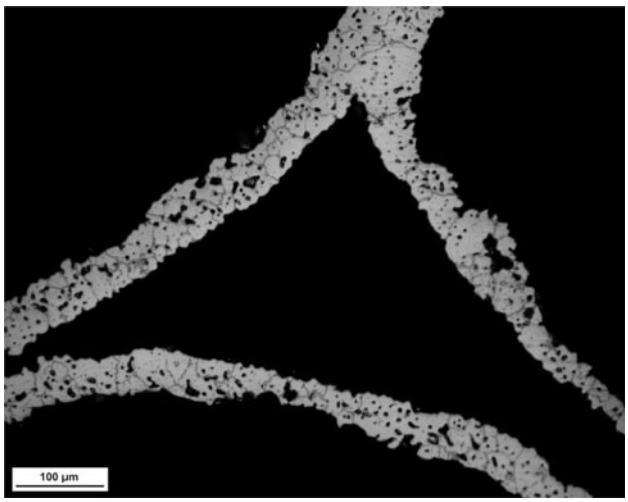

Fig. 2 Light optical micrograph of a sample showing the cell wall structure

Elastic analysis

Figure 3 shows typical amplitude and phase spectra for one sample each of Type A–C. The upper plot shows the amplitude spectra while the lower plot shows the phase spectra. In all three sample types, the amplitude spectra oscillate in a complex manner in the lower frequency regime. However, at the higher frequency regime, the signal drops beyond measurable limits. Experience shows that the signal becomes non-measurable when the amplitude typically drops below approx. −40 dB in the amplitude spectrum. For material Types B and C, this signal drop occurs at a frequency of approximately 500 kHz, while in material Type A, this occurs already at a frequency of about 250 kHz. In all samples, the measurement of sound velocity was carried out in this measureable lower frequency range. The ranges of measurable frequency in the three material types are marked in the phase spectra shown in Fig. 3. The phase spectra for Types B and C almost superimpose on each other until about 550 kHz. The lower plot of Fig. 3 shows that the slope of the individual phase spectrum is constant within this lower frequency range, suggesting that the sample is non-dispersive and the measured velocity is independent of frequency. Knowing the sample length and using the slope of the phase spectrum of each individual sample, the longitudinal sound wave velocity in each sample was determined using Eq. 1. Once this was measured, the longitudinal elastic constant C_{ii} of each sample was determined using Eq. 2.

For an isotropic material, C_{ii} is related to Young's modulus E via Poisson's ratio v according to the relation:

$$C_{ii} = \frac{E}{1 - \frac{2v^2}{1-v}} \tag{3}$$

As the individual spheres in the hollow sphere structure were arranged randomly, the material can be assumed to be

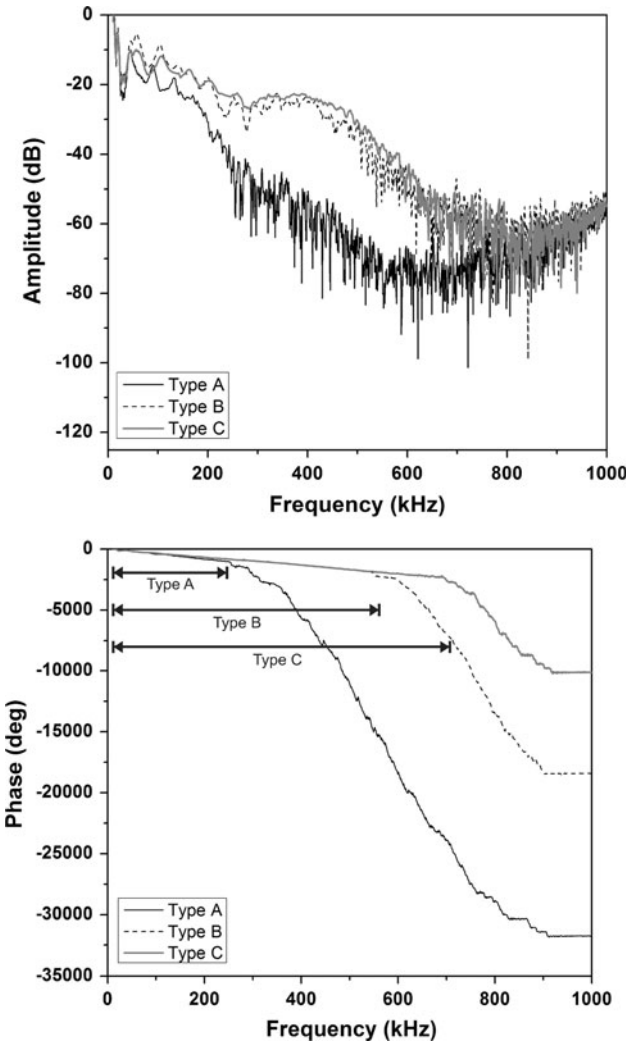

Fig. 3 Typical amplitude and phase spectra for one sample each of Type A–C. Phase spectra of Type B and Type C superimpose on each other until 550 kHz

isotropic. Poisson's ratio of the material was not known beforehand and determination of the exact value is difficult. Gibson and Ashby [7] have shown that for various materials and in both open and closed-cell foams, the Poisson's ratio is close to 0.33. This value was also used in the current work to compute the Young's modulus of each sample from the measured C_{ii}.

In Fig. 4, the experimentally determined relative Young's modulus of each sample taken from batches A, B, and C is compared with the theoretical predictions for open and closed-cell foams according to the GA model [7]. The Young's modulus of AISI 316L was taken as 193 GPa [16]. The plot shows that the experimental data points match well with the predictions for open-cell foams. This conclusion is consistent with the observation of Lim et al. [13]. They studied the mechanical properties of hollow sphere metal foams made of 405 stainless steel and showed

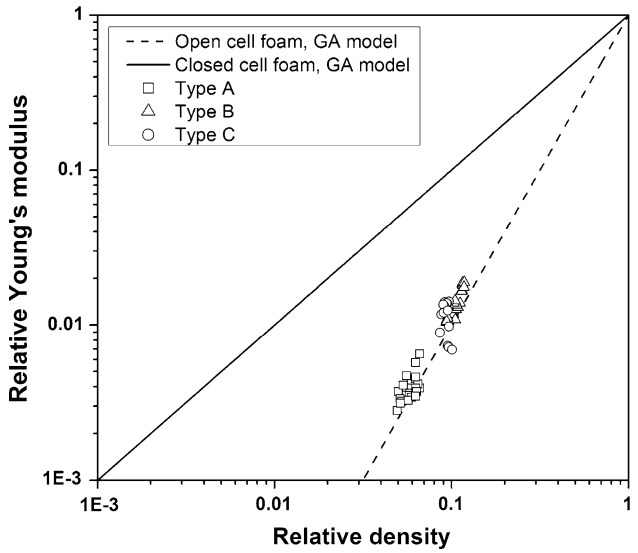

Fig. 4 Comparison of the experimentally determined Young's modulus of the hollow sphere samples using ultrasound phase spectroscopy with theoretical predictions for open and closed-cell foams

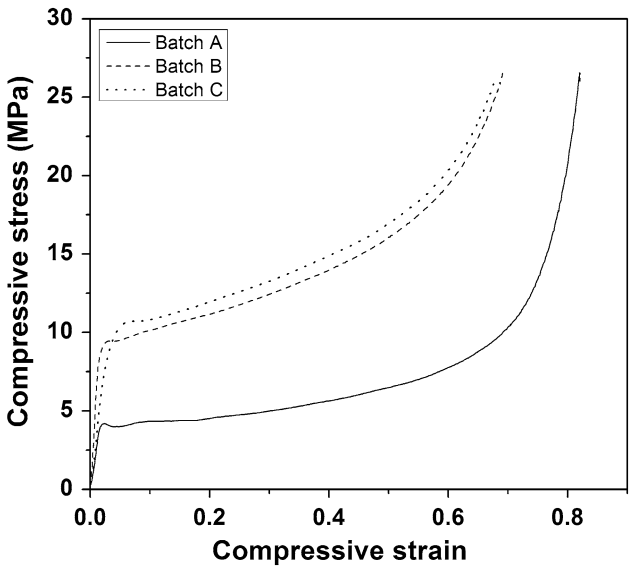

Fig. 5 Typical compressive stress–strain plots of the three material types at room temperature

that the foam stiffness lies close to the predictions of the theoretical open-cell structure.

Compression test

Figure 5 shows the typical compressive stress–strain plots at room temperature for one sample of each type at a strain rate of 10^{-3}/s. The plots are typical for cellular solids, showing a linear elastic region at the beginning, followed by an extended plateau region where the stress varies marginally with strain and finally a densification region where the stress–strain curve becomes almost vertical. Banhart and Baumeister [19] have summarized a few possible definitions for the plateau stress. Following Ref. [20], the average stress within 5–25% total strain range has been taken as the plateau stress. Calculated this way, plateau stresses for the three samples shown in Fig. 5 are 4.4 MPa (Type A), 11.4 MPa (Type B), and 10.6 MPa (Type C), respectively. Consistent with the predictions of the GA model [7], the plateau stress increases and the densification strain decreases with increasing relative density of the samples. As discussed by Lefebvre et al. [21], determination of the Young's modulus from the slope of the initial region of the compressive stress–strain plot of cellular solids typically yields significantly lower values due to the following reasons. At the beginning of the tests, non-linear deformation of the material is observed due to non-parallelism of the sample faces. This gives rise to inflexions in the compression stress–strain plots. Additionally, during sample loading, due to the heterogeneous structure of the material, load is not distributed uniformly and that causes localized plastic deformation at critically stressed regions. Accordingly, the slope of this combined elastic-plastically deforming material is significantly less than the real Young's modulus of the material. Young's modulus of the three samples shown in Fig. 5 was determined from the slope of the linear region of the respective stress–strain plots following the initial curved region resulting from sample non-parallelism. These values were found to be 4–8 times less than the Young's modulus determined by ultrasound phase spectroscopy. This results from the above mentioned effect of localized plastic deformation at regions of stress concentration. A more accurate value is obtained if the Young's modulus is determined by unloading the sample and measuring the slope of the unloading plot [22]. However, as the measurements are carried out on plastically deformed and possibly damaged specimens, even these values may be less than the actual Young's modulus of the sample [21]. To overcome this, Lefebvre et al. [21] measured the unloading Young's modulus of titanium foam samples at different levels of compressive deformation and then extrapolated the values to zero deformation to estimate the Young's modulus of undeformed specimens. Determination of Young's modulus from the compression stress–strain plots was not carried out in this work.

Figure 6 shows the effect of relative density on relative plateau stress (plateau stress normalized by the 0.2% yield stress of AISI 316L at room temperature) of the cellular hollow sphere structure. 0.2% yield stress of AISI 316L at room temperature was taken as 176 MPa [16]. Predictions following GA model for ideal open and closed-cell foams are shown as straight lines in the figure. The plot shows that at low relative densities the behavior of the hollow sphere

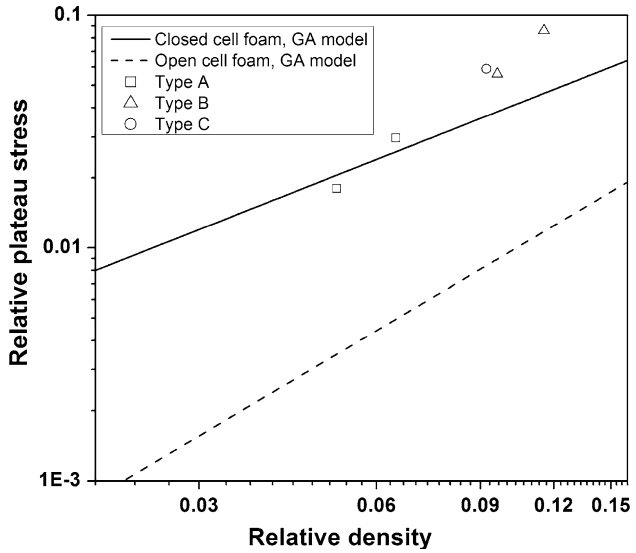

Fig. 6 Effect of the relative density on the relative plateau stress of the cellular hollow sphere structure

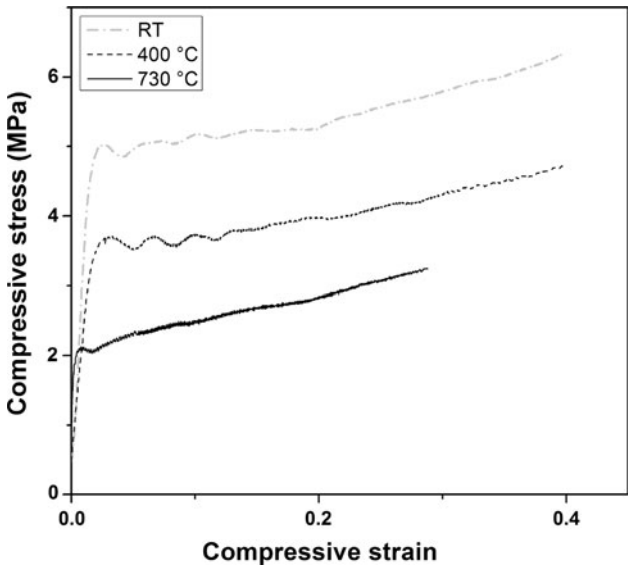

Fig. 7 Compressive stress–strain plots of samples of Type A at different temperatures

structure is similar to closed-cell foams, while at higher relative densities, they are even stronger. The accuracy of the trend shown by Fig. 6 is, however, limited by two factors. Firstly, the actual yield stress of the cell wall material of the hollow sphere structure is not known. An actual yield stress value significantly different from the value used in the current study will shift the theoretical lines for both open and closed-cell foams, without changing their slope. This change in yield stress may be caused by the presence of the microporosity in the cell walls, actual thermal conditions prevalent in the sample resulting from sintering and due to the actual chemical composition of the cell wall material. A more accurate value for the yield stress of the cell wall material can be obtained if bulk AISI 316L samples prepared from identical powders without the hollow spheres and sintered under identical conditions is compressed. Such identically fabricated bulk samples were, however, not available, and hence literature value for the yield stress of AISI 316L has been used in this work. Secondly, plateau stress of cellular solids is not a well defined parameter like the Young's modulus. In the GA model, the stress at which the extended plateau behavior initiates has been taken as the plateau stress. As shown in Fig. 5, the samples of Type A have a flat plateau, and hence, the chosen value of the plateau stress is not significantly different from the stress where the plateau initiates. However, the plateau region is rather steep in samples of Type B and Type C. As a result of this, the plateau stress as defined in the current study is located significantly higher than the point of plateau initiation.

Figure 7 shows compressive stress–strain plots of the samples of Type A at different temperatures. Compression tests were carried out at a strain rate of 10^{-4}/s. Samples of Type B and Type C displayed a similar trend and they are not shown here. The plot shows that, as expected, with increasing test temperatures, the overall level of the stress–strain curves decreases to lower stresses. The extended plateau visible at room temperature is also present at high temperatures. Figure 8 shows the effect of test temperature on the plateau stress (in log scale) of the three material types. For all the samples shown in the plot, the strain rate was 10^{-4}/s. For each material type, the best fit straight lines are also shown in the plot. The slopes of these best fit straight lines are similar, suggesting that the rate of decrease of the plateau stress with temperature is similar in

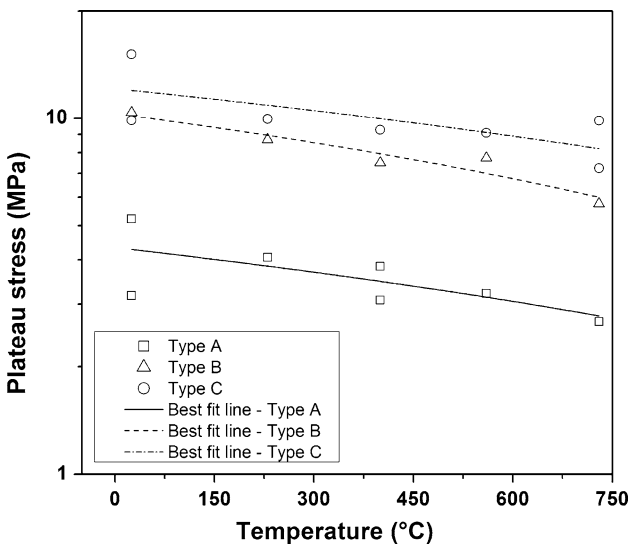

Fig. 8 Effect of test temperature on the plateau stress (in log scale) of the three material types

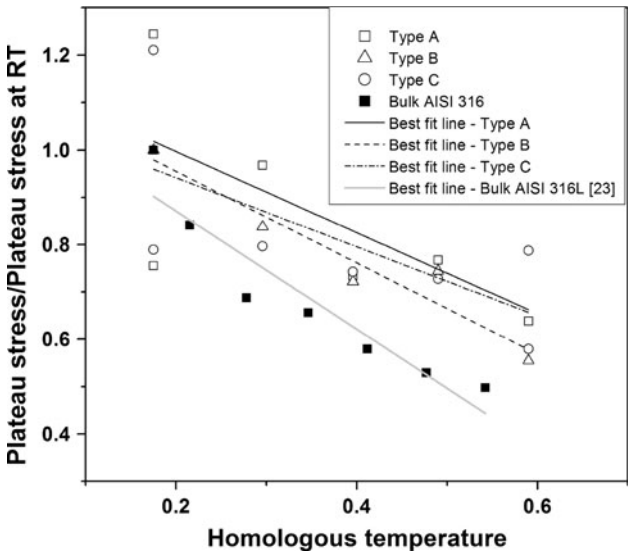

Fig. 9 Plot of the plateau stress at different temperatures normalized by the plateau stress at room temperature vs. homologous temperature. Solid squares correspond to the ratio of yield stress of AISI 316L at any temperature to the yield stress of AISI 316L at room temperature. Best fit straight lines for each material type are also shown

each material type. Figure 9 shows the ratio of the plateau stress at different temperatures to the plateau stress at room temperature plotted against the homologous temperature. If more than one sample for a particular material type was tested at room temperature, average plateau stress from these samples was used as the room temperature plateau stress for that type. To compare the temperature dependence of the plateau stress of the cellular hollow sphere structure with the temperature dependence of the strength of the bulk solid, data points for bulk AISI 316L are also shown in the same plot. These data points show the ratio of the 0.2% yield stress of AISI 316L at different temperatures to its room temperature yield stress. 0.2% yield stress of bulk AISI 316L at different temperatures has been taken from Ref. [23]. For both Type B and Type C, two samples were compressed at RT and their plateau stresses differed a lot, probably caused by their different relative densities. As, data points for individual samples are plotted in the figure, two data points (one each for Type B and Type C) at room temperature are located above the reference values of the bulk material. Straight lines shown in the diagram are the best fit lines for different material types. The plot shows that at high temperatures, the cellular hollow sphere solids are stronger than the base metallic alloy. Moreover, the rate of decrease of the strength with increasing temperature in the hollow sphere solids is also less than that in the bulk AISI 316L. However, due to the substantial scatter of the experimental results, the slightly better high temperature strength of the cellular material appears to be insignificant.

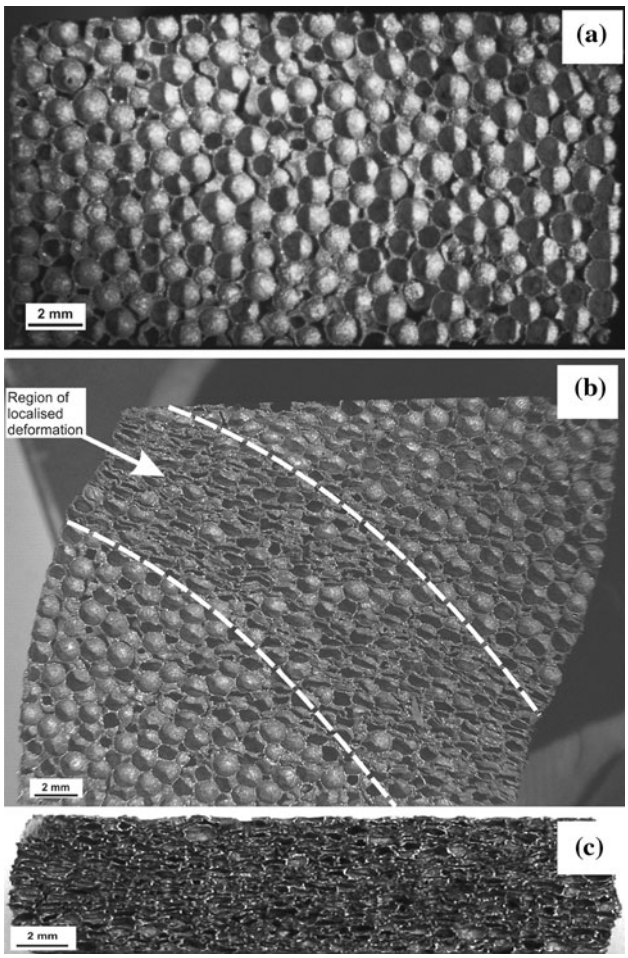

Fig. 10 Macroscopic section view of the face parallel to the direction of external compression: **a** undeformed sample, **b** sample compressed to a total strain ~ 0.4, and **c** sample compressed to a total strain of 0.8. Region of localized deformation is bounded by two white lines in image (**b**)

To observe the deformation mechanism, two samples of Type C compressed to different degrees of plastic deformation were chosen. One of the samples was deformed to a total strain of 0.4, and it was still in the plateau region. The second sample was deformed to a total strain of 0.8, and it had already been densified. The samples were sectioned by electric discharge machining (EDM) parallel to the loading direction and their photographs were taken. The images are shown in Fig. 10. For comparison, an image of an undeformed sample of the same Type is also shown in this figure. In Fig. 10b the heterogeneous nature of deformation within the plateau region can be clearly observed. The region marked by the arrow and bordered by the white lines is the region where the permanent deformation is localized and the regions away from this suffered little or no plastic deformation at all. A closer look into the picture shows the band-like propagation of deformation and that the cells within the band have collapsed. The deformation band

propagates along a direction of approximately 45° to the loading axis. Slight non-parallelism of the opposite faces of the compressive samples may cause early initiation of localized shear within the sample. This non-parallelism of the opposing sample faces also gives rise to inflexions at the beginning of the compression stress–strain plots. Effect of this non-parallelism is cancelled once the opposing faces become parallel to each other and the stress–strain plot becomes linear. Closer look into the initial portion of the stress–strain plots of Fig. 5 shows that the curves become linear already at a total strain of approximately 1%. Observation of the shear band-like deformation propagation at a total strain as high as 40% is caused by the shearing of individual spheres over each other. Figure 10c shows the photograph of one sample deformed to a strain of 0.8. No elastic region can be observed here and the propagation of deformation is homogeneous throughout the sample. All the cells have collapsed and the structure has densified.

Conclusions

Cellular solids produced from hollow stainless steel spheres were studied in this work. Longitudinal elastic constant was determined at room temperature with the help of ultrasound phase spectroscopy. Mechanical tests were carried out under external compression up to a homologous temperature of 0.6. The following conclusions can be drawn:

- Dependence of the relative Young's modulus on the relative density of the hollow sphere structure is similar to that shown by conventional open-cell foams.
- Compressive stress–strain curves showed the three distinct regions of linear elasticity, plateau and densification. Within the plateau region the deformation proceeded in the form of bands at 45° to the loading axis with cells within the bands undergoing permanent deformation and cells away from it experiencing only elastic deformation. Plateau stress increased and densification strain decreased as the sample density increased. Due to the uncertainties related to the properties of the bulk alloy and the definition of the plateau stress, it cannot be determined whether the open or closed-cell version of the GA model accurately predicts the experimental data.
- With increase in test temperature the overall level of the compressive stress–strain plots shifted to lower stresses. The rate of decrease of the plateau stress with increasing temperature was independent of sample density. The hollow sphere solids showed slightly better high temperature strength in comparison to the base metal. However, due to the considerable scatter in the experimental data points, this improvement seems to be insignificant.

Acknowledgements Co-author SR is grateful to DAAD (Deutscher Akademischer Austausch Dienst) for funding his stay in Karlsruhe, Germany under DAAD—Masters sandwich Model Scholarship and thanks Prof. B. P. Kashyap (Department of Metallurgical Engineering and Materials Science, IIT Bombay) for his guidance and for introducing him to the topic of metallic foams. The authors also thank Dr. K. A. Weidenmann (IAM-WK, KIT) for cross-reading the manuscript and for giving valuable suggestions.

References

1. Banhart J (2001) Prog Mater Sci 46:559
2. Stephani G, Andersen O, Göhler H, Kostmann C, Kümmel K, Quadbeck P, Reinfried M, Studnitzky T, Waag U (2006) Adv Eng Mater 8:847
3. Ashby MF, Evans A, Fleck NA, Gibson LJ, Hutchinson JW, Wadley HNG (2000) Metal foams, a design guide. Elsevier Science, USA
4. Miyoshi T, Itoh M, Akiyama S, Kitahara A (2000) Adv Eng Mater 2:179
5. Korner C, Singer RF (2000) Adv Eng Mater 2:159
6. Stöbener K, Rausch G (2009) J Mater Sci 44:1506. doi: 10.1007/s10853-008-2786-8
7. Gibson LJ, Ashby MF (1988) Cellular solids, structure and properties. Cambridge University Press, UK
8. Sanders WS, Gibson LJ (2003) Mater Sci Eng A352:150
9. Waag U, Schneider L, Löthman P, Stephani G (2000) Met Powder Rep 33:29
10. Friedl O, Motz C, Peterlik H, Puchegger S, Reger N, Pippan R (2008) Met Mater Trans 39B:135
11. Lhuissier P, Fallet A, Salvo L, Brechet Y (2009) Mater Lett 63:113
12. Fallet A, Lhuissier P, Salvo L, Brechet Y (2008) Adv Eng Mater 10:858
13. Lim T-J, Smith B, McDowell DL (2002) Acta Mater 50:2867
14. Sanders WS, Gibson LJ (2003) Mater Sci Eng A347:70
15. Gasser S, Paun F, Cayzeele A, Bréchet Y (2003) Scr Mater 48:1617
16. ASM International (1996) ASM specialty handbook on stainless steels. Materials Park, Ohio, USA
17. Wanner A (1998) Mater Sci Eng A248:35
18. Scott GD, Kilgour DM (1969) J Phys D 2:863
19. Banhart J, Baumeister J (1998) J Mater Sci 33:1431. doi: 10.1023/A:1004383222228
20. Haag M, Wanner A, Clemens H, Zhang P, Kraft O, Arzt E (2003) Met Mater Trans 34A:2809
21. Lefebvre L-P, Blouin A, Rochon S-M, Bureau MN (2006) Adv Eng Mater 8:841
22. Sugimura Y, Meyer J, He MY, Bart-Smith H, Grenstedt J, Evans AG (1997) Acta Mater 45:5245
23. Spaeder CE, Domis WF, Brickner KG (1973) High-nitrogen austenitic stainless steels. ASTM STP 522, American Society for Testing Materials, p 35